THE JOURNAL OF PHYSICAL CHEMISTRY LETTERS
A JOURNAL OF THE AMERICAN CHEMICAL SOCIETY

pubs.acs.org/JPCL

Letter

# $OH^-\cdots$Au Hydrogen Bond and Its Effect on the Oxygen Reduction Reaction on Au(100) in Alkaline Media

Yuke Li, Yan-Xia Chen,* and Zhi-Feng Liu*

Cite This: J. Phys. Chem. Lett. 2022, 13, 9035−9043

Read Online

ACCESS | Metrics & More | Article Recommendations | Supporting Information

**ABSTRACT:** Using ab initio molecular dynamics simulations with fully solvated ions, we demonstrate that solvated $OH^-$ forms a stable hydrogen bond with Au(100). Unlike the hydrogen bond between $H_2O$ and Au reported previously, which is more favorable for negatively charged Au, the $OH^-\cdots$Au interaction is stabilized when a small positive charge is added to the metal slab. For electro-catalysis, this means that while $OH_2\cdots$Au plays a significant role in the hydrogen evolution reaction, $OH^-\cdots$Au could be a significant factor in the oxygen reduction reaction in alkaline media. It also points to a fundamental difference in the mechanism of oxygen reduction between gold and platinum electrodes.

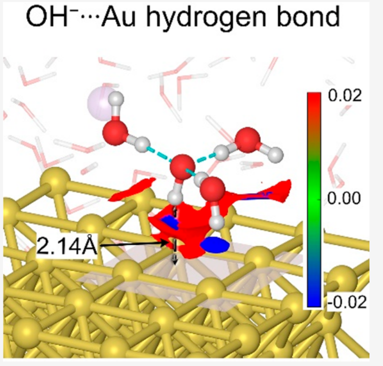




Hydrogen bonding typically occurs between a hydrogen atom and an electronegative non-metal atom such as O, N, F, or Cl or their anions as the hydrogen bond acceptor. A transition metal atom serving as an acceptor represents an unconventional type of hydrogen bond,[1,2] as indicated by a short XH$\cdots$M distance in organometallic complexes. Gold has been a prominent example of such a hydrogen bond acceptor because it is the most electronegative metal element, with a high electron affinity and small atomic and/or ionic radii due to relativistic contraction.[3,4] Its unconventional nature is indicated by the fact that clear evidence for such a hydrogen bond was first obtained in the cases of NH$\cdots$Au[5−7] and CH$\cdots$Au,[8,9] while the identification of the OH$\cdots$Au hydrogen bond has been more challenging.[3] Theoretically, a negatively charged $Au^-$ in $AuMe_2^-$ solvated by $H_2O$ via HOH$\cdots Au^-$ has been demonstrated,[10−12] similar to the $Au^-(H_2O)$ anionic cluster examined in the gas phase by photoelectron spectroscopy.[13,14] Experimentally, the OH$\cdots$Au hydrogen bond has been determined only very recently in gold(I) indazol-3-ylidene complexes by X-ray diffraction, nuclear magnetic resonance, and vibrational spectroscopy.[15]

Similar interactions between water molecules and the surface metal atoms of an electrode have also been studied in electrochemistry.[16,17] Via application of a potential negative of its potential of zero charge (PZC), surface atoms on a metal electrode such as Cu, Ag, and Au can become negatively charged. Significant changes in the vibrational modes of adsorbed water molecules were detected by surface-enhanced Raman spectroscopy[16,18] and infrared absorption spectroscopy[19] and attributed to the hydrogen bonding interaction, HOH$\cdots$M. In the case of a Au electrode, there was evidence that as the electrode potential became more negative, an interfacial water molecule could evolve from a structure with one H pointing to the surface to a structure with both hydrogen atoms pointing to the surface.[20] As they require a negative electrode potential, such interactions play a significant role in electro-catalysis for the hydrogen evolution reaction (HER).[21] It is in contrast to another common type of interaction between the oxygen end of water and a metal atom, $H_2O\cdots$M, which are dominant at positive electrode potentials in the active range for the oxygen reduction reaction (ORR).

In this paper, we report an ab initio molecular dynamics (AIMD) study of explicitly solvated $OH^-$ in an aqueous interfacial environment near an electrode of Au(100) and demonstrate another unusual type of hydrogen bonding, between $OH^-$ and a Au(100) surface, in the ORR potential region. The hydrogen bond donor $OH^-$ has very low acidity, while the $OH^-\cdots$Au hydrogen bond is stabilized by a small positive electrode potential. Such a hydrogen bond makes the mechanism of ORR on Au(100) fundamentally different from that on Pt(111) in an alkaline environment.

Included in our models are a Au(100) slab mimicking an electrode surface, 48 water molecules, and a NaOH molecule that automatically dissociates into a sodium ion ($Na^+$) solvated in the solution layer and a hydroxide ($OH^-$) ion, either in the

**Received:** September 8, 2022
**Accepted:** September 20, 2022
**Published:** September 23, 2022




https://doi.org/10.1021/acs.jpclett.2c02774
J. Phys. Chem. Lett. 2022, 13, 9035−9043

solution layer or on the slab surface as adsorbed OH*. As demonstrated in our previous study of Pt(111), such a model with fully solvated electrolyte ions is essential for understanding the impact of solvation dynamics on the ORR mechanisms.[22−24]

When it comes to solvated $OH^-$, the results on Au(100) are in striking contrast with the results on Pt(111). As shown in Figure 1a for a NaOH|Pt(111)|$nH_2O$ model, the $OH^-$

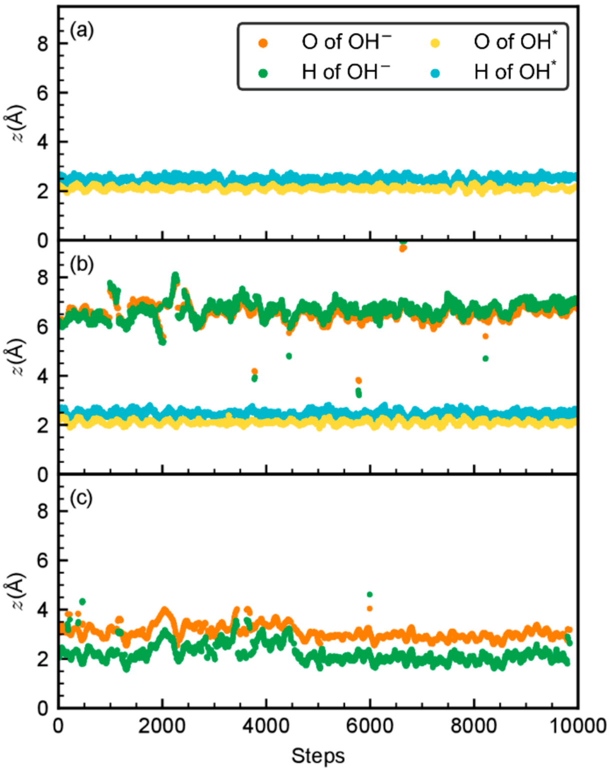


**Figure 1.** Time evolution of the $z$ coordinates of O and H for $OH^-$/OH* during AIMD simulations at 300 K. As the normal of the metal surface is along the $z$ direction and the $z$ coordinate of the surface is set to 0, the $z$ coordinate for an atom is its distance to the metal surface. (a) In a NaOH|Pt(111)|$nH_2O$ model, OH* is adsorbed on Pt(111) with its oxygen end. (b) In a 2NaOH|Pt(111)|$nH_2O$ model, one OH* is adsorbed and one $OH^-$ is in the solution layer. (c) In a NaOH|Au(100)|$nH_2O$ model, $OH^-$ is in the solution layer, with the H end pointing to the Au(100) surface.

produced by the ionic dissociation of NaOH is adsorbed on Pt(111) as OH* (surface species are indicated by asterisks hereafter). In our model, the surface normal lies along the $z$ direction and the reported $z$ coordinate is relative to the top layer surface Au atoms and therefore equal to the distance to the surface. As the bonding interaction is between O and Pt, the OH bond is slightly tilted up from the surface, indicated by the slightly larger $z$ value for H than for O. Within this model, it is hard to desorb OH*, which could be achieved only by adding −1.0e or more negative charge to the Pt(111) slab.[24] However, after the addition of one more NaOH to afford a 2NaOH|Pt(111)|$nH_2O$ model, one $OH^-$ is typically observed in the solution layer while the other $OH^-$ would stay on the surface as OH* (Figure 1b). The position of the solvated $OH^-$ is often >6 Å above Pt(111), clearly in the outer sphere region, and does not come near the surface during the AIMD simulation of 10 000 steps (12.0 ps).

In contrast, no extra negative charge or extra cation is needed to observe a solvated $OH^-$ in the interfacial region on top of Au(100), using a NaOH|Au(100)|$nH_2O$ model (Figure 1c). Furthermore, as the $z$ value of H is smaller than the $z$ value of O by ∼1 Å, it is obvious that this $OH^-$ is pointed to the surface with its H end, almost vertically, because the O−H bond distance is ∼1 Å. Finally, the H end of $OH^-$ is very close to Au(100), with a distance just above 2.0 Å.

Shown in Figure 2 is a typical optimized structure for the NaOH|Au(100)|$nH_2O$ model. The $OH^-$, as a hydrogen bond

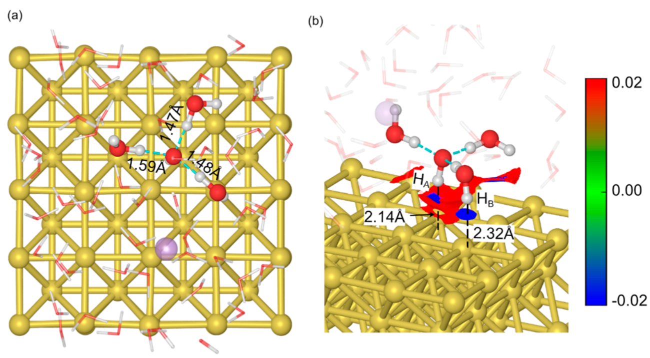


**Figure 2.** Optimized structure of the NaOH|Au(100)|$nH_2O$ model. (a) Top view, showing the hydrogen bonds accepted by $OH^-$ from three $H_2O$ molecules in its first solvation shell. (b) Side view, showing the noncovalent interaction plot with blue and red indicating attractive and repulsive interaction, respectively.

acceptor, is solvated by three water molecules forming its first solvation shell. The lengths of these hydrogen bonds (1.47, 1.48, and 1.59 Å) indicate strong solvation interactions, similar to the first-shell hydrogen bonds reported previously for $OH^-(H_2O)_n$ clusters.[25] Bader population analysis[26] shows that the negative charge is indeed on $OH^-$ (−0.71e) and the positive charge is on $Na^+$ (0.84e), while the charge on the Au(100) slab is only 0.04e. The calculated electron localization function[27] also indicates no covalent bonding interaction between $OH^-$ and the Au surface (see Figure S1). However, a noncovalent interaction (NCI)[28,29] plot does indicate the presence of two OH···Au hydrogen bonds, one between $OH^-$ and Au (through $H_A$) and another between $H_2O$ and Au (through $H_B$).

Both $OH^-$ and this $H_2O$ molecule are close to the surface. For $OH^-$, the $H_A$−surface distance is 2.14 Å, and for the $H_2O$, the $H_B$−surface distance is 2.32 Å. However, the distance to the surface is not the same as the H···Au distance that further depends on the adsorption site. $H_B$ is on a top site, interacting with one Au atom. The $H_B$···Au distance is 2.39 Å, only slightly larger than its distance to the surface, and the O−$H_B$−Au angle is 155°, fitting well with the definition of a typical HOH···Au hydrogen bond.[12] In contrast, $H_A$ (of $OH^-$) is on a bridge site, interacting with two Au atoms. The $H_A$···Au distances are 2.70 and 2.79 Å, ∼0.6 Å larger than its distance to the surface, and the O−$H_A$−Au angles are 155° and 138°, similar to the hydrogen bond to Au atoms reported for coordinated gold clusters.[8]

The application of an electrode potential, which is simulated in our model by adding an extra charge to the Au(100) slab, could disturb this $OH^-$···Au interaction. Using the double-reference method developed by Neurock and co-workers,[30,31] we estimate the shift in the electrode potential caused by adding a charge of 1.0e is ∼0.5 V for our model (see Figure


https://doi.org/10.1021/acs.jpclett.2c02774
J. Phys. Chem. Lett. 2022, 13, 9035−9043

S2). As shown in panels a and b of Figure 3, the $OH^-\cdots Au$ hydrogen bond is largely preserved when a charge of −0.5e or

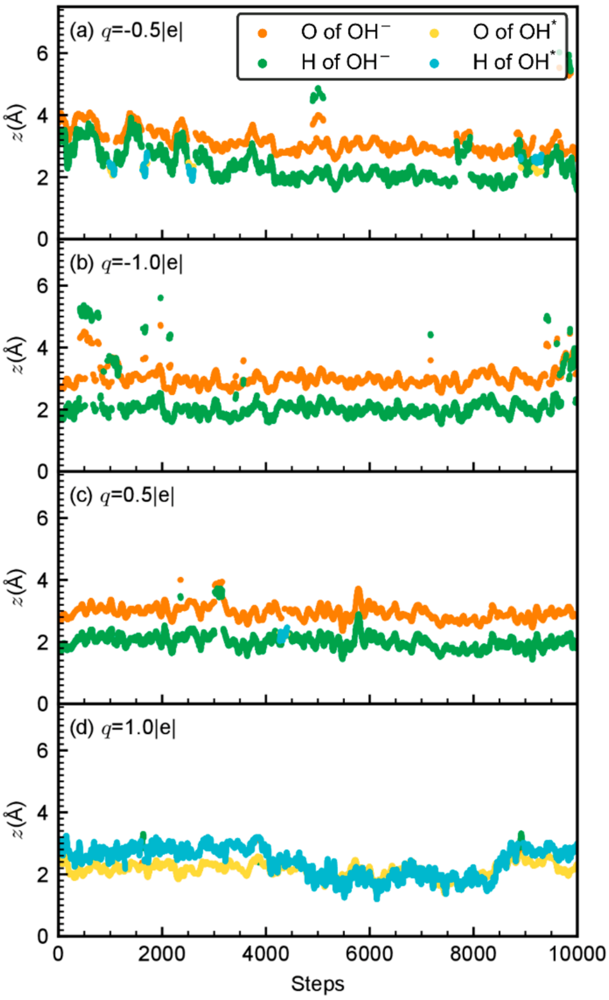


**Figure 3.** Time evolution of the $z$ coordinates of O and H for $OH^-$/$OH^*$ during AIMD simulations at 300 K for a NaOH|Au(100)|$n$$H_2O$ model, with charge $q$ added to the slab.

−1.0e is added, corresponding to a shift of −0.25 or −0.5 V, respectively, from the potential of zero charge (PZC) at 0.33 V (SHE) for Au(100).[32,33] When $q$ = −0.5e, the $OH^-$ sometimes moves into the solution layer, with the H atom >3 Å from the Au surface, and sometimes adsorbs on the Au(100) surface (Figure 3a). When $q$ = −1.0e, $OH^-$ could sometimes move to >4 Å from the surface, showing up in Figure 3b as jumps in the $z$ coordinates because such movement is always achieved by proton transfer. The solvated $OH^-$ could also change its orientation during such jumps, with the $z$ coordinate of H being larger than that of O.

On the contrary, when a charge of 0.5e is added [an approximately +0.25 V shift from the PZC (Figure 3c)], the $OH^-\cdots Au$ hydrogen bond is strengthened, as indicated by an average $z$ for the H atom of 2.23 ± 0.38 Å for $q$ = 0e being reduced to 2.02 ± 0.28 Å for $q$ = 0.5e during the respective AIMD runs. This observation is contrary to the expectation that positive charge on a Au atom would make it less a hydrogen bond acceptor. Finally, when a charge of 1.0e is added [an approximately +0.5 V shift from the PZC (Figure 3d)], the $OH^-\cdots Au$ hydrogen bond does not survive the equilibration run, as its orientation is flipped to become an adsorbed $OH^*$. With its oxygen end bonding to a Au atom, this is the typical oxidation interaction expected on a metal surface in the ORR region.

Shown in Figure 4a−e are the $z$ distribution functions for the H atom of $OH^-$/$OH^*$ and $H_2O$ with varying $q$ values. For the H atom of $H_2O$, the first peak just above 2.0 Å at $q$ = −1.0e indicates there are hydrogen bond interactions between some of the $H_2O$ molecules and Au atoms on the Au(100) surface (Figure 4a). This peak is gradually reduced as the value of $q$ changes to −0.5e, 0.0e, 0.5e, and 1.0e, in agreement with the expectation that such hydrogen bonds would be weakened at zero and positive electrode potentials.[16,20,34] For the H atom of $OH^-$, there is a well-resolved peak around 2.0 Å at $q$ = 0.5e. This peak is broadened at $q$ = 0.0e and −0.5e and is well resolved again at $q$ = −1.0e, albeit with small tails at high $z$ values. When $q$ = 1.0e, $OH^*$ is adsorbed on a top site and the bending of the Au−O−H angle shows up as the fluctuation of the $z$ value between 1.5 and 3.0 Å (Figure 4e).

When the radial distribution functions of Au atoms around the H atom of $OH^*$/$OH^-$ are plotted in Figure 4f−j, it is obvious that there is no hydrogen bonding interaction between $OH^*$ and Au, as the first Au peak is at 2.92 Å (Figure 4j). In contrast, the first Au peak for $q$ = 0.5e is at 2.46 Å (Figure 4i), clearly within the range of $OH^-\cdots Au$ hydrogen bonds. When $q$ = 0.0e, − 0.5e, and −1.0e, the position of the first Au peak is slightly increased, while there is always a second Au close to 3 Å, indicating a bridge position.

While the $OH^-\cdots Au$ hydrogen bond holds up very well during the 300 K AIMD simulations when $q \leq 0.5$e, it is nontrivial to estimate its binding energy in a fully solvated model. There are many flexible hydrogen bonds in the system, and optimized structures could produce only local minima. During AIMD simulations, it is impossible to force the $OH^-$ at a particular location as it can easily move around the solution layer upon proton transfer. By using a frozen $NaOH(H_2O)_{14}$ cluster with $OH^-(H_2O)_3$ at its tip, we estimate the hydrogen bond interaction energy between a hydrated $OH^-$ and Au(100) is 11−14 kcal/mol when the H of $OH^-$ is 2.0−2.4 Å above the surface (see Figure S3 and Table S1), in line with the previously reported binding energy of 10 kcal/mol for the $HOH\cdots Au^-$ cluster.[17]

In hydrogen bonding interactions, $OH^-$ is best known as a strong acceptor through its O end, rather than a donor through its H end.[35,36] In small hydrated clusters, $OH^-(H_2O)_n$, the first solvation shell usually contains three hydrogen bonds, similar to the structure shown in Figure 2, with distances of ∼1.6 Å and incremental association enthalpies of −27.0, −20.1, and −16.9 kcal/mol for $n$ = 1, 2, and 3, respectively.[25] These are bonding energies much stronger than that for a typical hydrogen bond of ∼5 kcal/mol between two $H_2O$ molecules. On the contrary, the hydrogen end of an $OH^-$ is a weak hydrogen bond donor, and $OH^-$ would stay on the cluster surface with its H unsolvated and dangling.[37,38] Only when $n$ reaches ≥20 does it become possible for the hydrogen end of $OH^-$ to be buried inside a cluster during part of the AIMD simulations.[39,40] Experimentally, it has been determined that $OH^-$ can be a donor in a hydrogen bond, albeit such a hydrogen bond is relatively weak.[41−43] In our NaOH|Au(100)|$n$$H_2O$ model, $OH^-$ is also well solvated at its O end by water molecules and positioned at the edge of the solution phase, next to the Au surface. However, the hydrogen end of $OH^-$ can now interact with surface Au atoms and form a relatively


https://doi.org/10.1021/acs.jpclett.2c02774
J. Phys. Chem. Lett. 2022, 13, 9035−9043

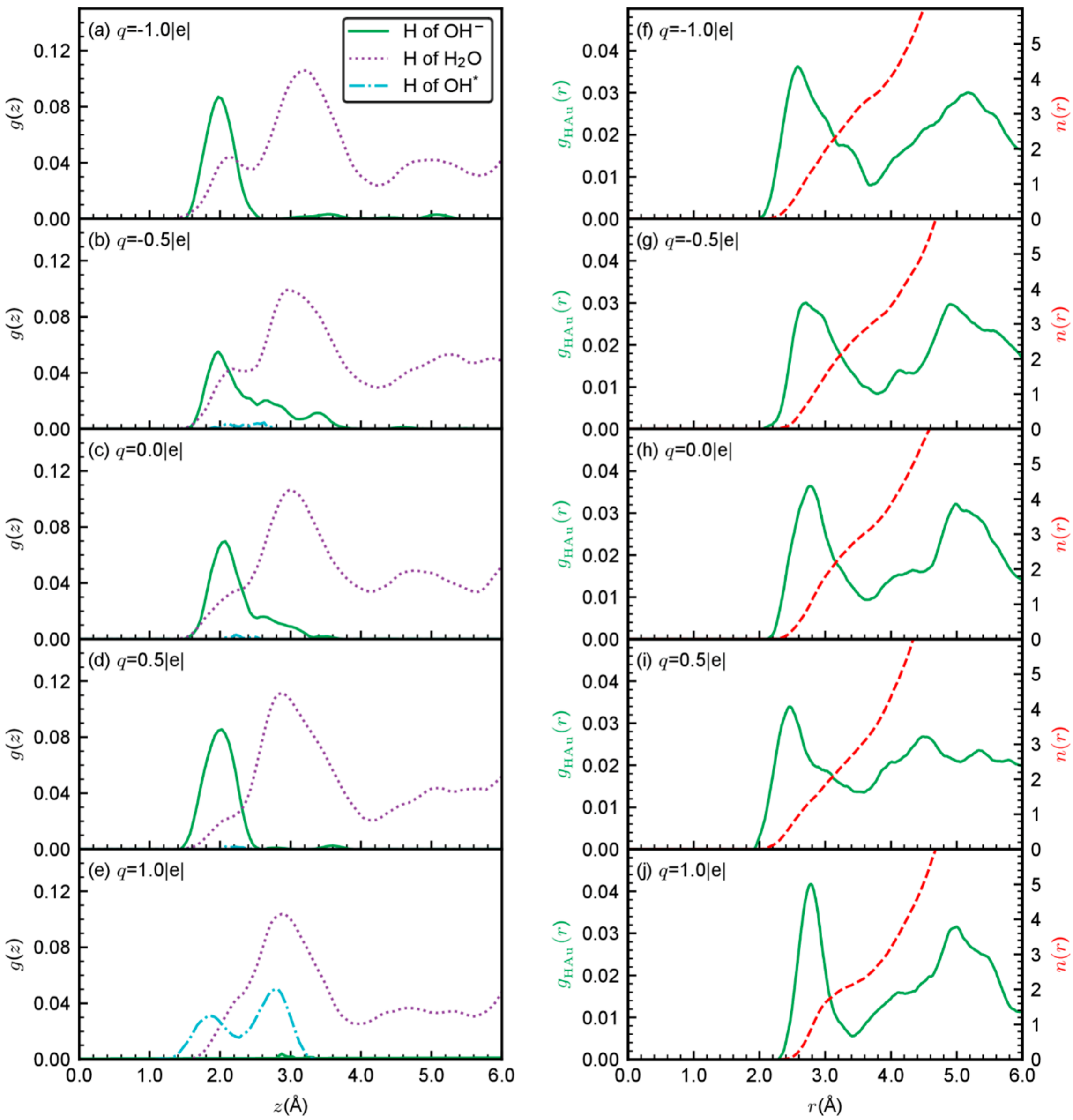


**Figure 4.** (a–e) $z$ distribution functions for H from $OH^-$, OH*, and $H_2O$ obtained from AIMD simulations at 300 K with various charges. For the H from $H_2O$, the function is scaled by 1/10. (f–j) Radial distributions of Au atoms around the H atom of $OH^-$ or OH* at various charges (green) and the integrated number of atoms, $n(r)$, from 0 to $r$ (red). The simulation model is a NaOH|Au(100)|$n$$H_2O$ model.

strong $OH^-\cdots$Au hydrogen bond with a binding energy of ~10 kcal/mol.

That such a hydrogen bond is the shortest and fluctuates the least on a 0.5e charged slab is quite unexpected, as is the observed trend that its distance to the surface and its fluctuation increase as the slab charge becomes more negative. A hydrogen bond should be strengthened when the acceptor, in this case a surface Au atom, becomes more negatively charged. In electrochemistry, this can be achieved by applying a negative potential to an electrode, which would increase the negative charge on surface metal atoms and strengthen the interactions with the hydrogen ends of water molecules, as indeed observed in many studies.[16−20]

To examine the charge on the surface Au atom interacting with $OH^-$, we performed charge analysis by the Bader scheme on each of the optimized structures for the NaOH|Au(100)|$n$$H_2O$ model with $q$ = 0.5e, 0.0e, −0.5e, and −1.0e. These structures have been used as the starting configurations for the AIMD simulations shown in Figures 1 and 3. In all cases, the $OH^-\cdots$Au hydrogen bond is on a bridge site, involving a pair of surface Au atoms. For $q$ = 0.5e and 0.0e, both surface Au atoms are negatively charged, ranging from −0.04e to −0.09e. In contrast, for $q$ = −0.5e and −1.0e, only one surface Au atom is negatively charged (−0.06e/−0.03e) while the other is slightly positively charged (both at 0.02e). This is in agreement with the results of AIMD simulations showing that the $OH^-\cdots$Au hydrogen bond is stronger for $q$ = 0.5e and 0.0e than for $q$ = −0.5e and −1.0e, but it raises the question of why the two surface Au atoms directly involved in the $OH^-\cdots$Au hydrogen bonding are less negative, when the overall slab charge is actually more negative.

The answer lies in the uneven distribution of charge on the surface, which can be influenced by the interfacial solution layer. As the slab becomes more negatively charged, the hydrogen bonding interactions between $H_2O$ molecules and surface Au atoms are enhanced. Correspondingly, there is an


https://doi.org/10.1021/acs.jpclett.2c02774
J. Phys. Chem. Lett. 2022, 13, 9035−9043

increase in the number of HOH⋯Au hydrogen bonds, which is clearly seen in Figure 4a−d, as well as in previous studies.[18,20] With more surface Au atoms taking up negative charge for interactions with $H_2O$, there is less negative charge on the surface bridge site for $OH^-$⋯Au hydrogen bonding. Unlike the neutral $H_2O$, $OH^-$ is an anion, and its Coulomb interaction with a negatively charged slab is repulsive, which also exerts a force on it, pointing away from the surface.

The situation is reversed when the slab is positively charged. The overall Coulomb interaction between $OH^-$ and a positively charged slab is now attractive, pulling $OH^-$ toward the surface, while the HOH⋯Au hydrogen bond is unfavorable. $H_2O$ molecules would interact with surface Au atoms with their O ends, pushing electrons away from these Au atoms. The redistribution of charge could then make the surface bridge site more negative for $OH^-$⋯Au hydrogen bonding. It is the charge on individual surface Au atoms, rather than the overall slab charge, that is responsible for the shortest $OH^-$⋯Au distance observed on a 0.5e charged slab. The electrode potential at $q$ = 0.5e, estimated from the double-reference method, is close to 0.6 V (a PZC of 0.33 V[32,33] and a further approximately +0.25 V shift due to the slab charge) and falls in the ORR region. As our AIMD simulations are performed under the condition of constant charge, such a potential is only an approximate estimate,[44] but counter-intuitive as it may be, there are physical reasons for the strengthening of the $OH^-$⋯Au hydrogen bond on a positively charged slab.

Despite changes in slab charges, the $OH^-$⋯Au hydrogen bond is generally maintained during AIMD simulations, from $q$ = −1.0e to 0.5e, with the solvated $OH^-$ staying in the first layer above Au(100). Only during very short durations would $OH^-$ move to the outer sphere, for $q$ = −1.0e and −0.5e, as shown in panels a and b of Figure 3. Without such a hydrogen bond with surface metal atoms, $OH^-$, as a strong hydrogen bond acceptor in its interactions with water molecules, would be better solvated in the outer sphere, away from the surface, as demonstrated in the case of Pt(111)[24] (also see Figure 1b).

The stability of the $OH^-$⋯Au hydrogen bond could be extended further into the higher-potential region. For our model with 48 Au atoms, the electrode potential is increased by 0.5 V when a charge of 1.0e is added. The average charge on each Au atom is fairly small, while the distribution is not uniform. The interactions with solvent and adsorbed molecules could produce both slightly positive and slightly negative surface Au atoms. However, further into the high-potential region, there is a new factor to consider: bonding between the oxygen end of $OH^-$ and a surface Au atom, Au−OH, would become more favorable than $OH^-$⋯Au interaction. In an alkaline medium, it leads to the adsorption of $OH^-$ on an electrode surface as OH*.

We observe such a transformation from $OH^-$⋯Au to Au−OH at $q$ = 1.0e. The electrode potential estimated by the double-reference method is ∼0.8 V (PZC of 0.33 V plus a +0.5 V shift). However, the beginning of OH* does not mean the end of $OH^-$⋯Au. The chemisorption of an anion could bring negative charge to the electrode surface.[45] Our charge analysis shows that at $q$ = 1.0e there are still negatively charged Au atoms around the OH* adsorption site, which could interact with solvated $OH^-$ via hydrogen bonding. The initial adsorption of $OH^-$ is the beginning of a new phase with a mixture of OH* and $OH^-$⋯Au, although a detailed investigation would require a larger model with additional NaOH. Nonetheless, the experimentally measured equilibrium potential on Au(100) between $OH^-$ adsorption and OH* desorption is actually ∼1.1 V (RHE).[46] This indicates that $OH^-$ is energetically more favorable than OH* up to 1.1 V, and therefore, an $OH^-$⋯Au hydrogen bond could be present in that potential range, as well.

The ORR mechanism on Au(100) in an alkaline medium is not yet fully understood.[47] There are good arguments that the initial step of electron transfer to $O_2$ is an outer sphere process and limits the ORR rate.[47,48] Below 0.6 V (RHE), it is a two-electron reduction, with $OOH^-$ produced, while above 0.6 V, it becomes a four-electron reduction, with $OH^-$ being the final products. The rate in the four-electron region is actually better than the ORR rate on Pt(111) in an alkaline medium.[46] There is evidence that the presence of water would promote the production of OH*.[49,50] This means the production of $OH^-$ should be due to OH* desorption.

In the case of the alkaline ORR on Pt(111), we previously demonstrated by AIMD simulations that the equilibrium

$$OH^* + e^- \rightleftharpoons OH^- \tag{1}$$

determines its ORR onset potential.[24] Above this potential, $OH^-$ would adsorb on the surface, and even the energetically most favorable reduction step

$$O^* + H_2O + e^- \rightarrow OH^* + OH^- \tag{2}$$

would be followed by $OH^-$ adsorption, making the overall process an electrochemically inactive one

$$O^* + H_2O^* \rightarrow 2OH^* \tag{3}$$

and turning off the reduction current.

Furthermore, as the solvation interaction between $OH^-$ and $H_2O$ is strong, reaction 1 is achieved by an indirect process[24]

$$OH^* \cdots (H_2O)_n \cdots H_2O + e^- \rightarrow {}^*OH_2 \cdots (H_2O)_n \cdots OH^- \tag{4}$$

For OH* desorption, this means OH* would pick up a proton from the solvation layer and become an adsorbed $H_2O^*$, while an $OH^-$ is produced in the solvation layer. It is a cross sphere reaction, involving the inner and outer spheres, facilitated by the transfer of a proton through two or three layers of water molecules, so that the product $OH^-$ is well solvated.

This physical picture is fundamentally changed on Au(100), when the $OH^-$ can be stabilized by hydrogen bonding with surface Au atoms. The product of OH* desorption is now in the inner sphere, stabilized by an $OH^-$⋯Au hydrogen bond. The observed reaction during our meta-dynamics simulations, with Au−OH* as the reaction coordinate, is

$$Au{-}OH^* \cdots OH_2 + Au' + e^- \rightarrow Au + OH_2 \cdots OH^- \cdots Au' \tag{5}$$

The activation barrier is only around 0.1−0.2 eV (see Table S2). More importantly, the process is now an inner sphere reaction, rather than a cross sphere reaction.

Markovic and co-workers have shown that the ORR rates on Pt(111) and Au(100) differ in their sensitivity to the cation identity. On Pt(111), the ORR rate varied in an alkaline MOH solution when $M^+$ was changed ($Cs^+ > K^+ > Na^+ \gg Li^+$), even though these cations, being solvated in the solution layer, could have only noncovalent interactions with the electrode surface.[51] On the contrary, they observed no such effects for



https://doi.org/10.1021/acs.jpclett.2c02774
J. Phys. Chem. Lett. 2022, 13, 9035−9043

the alkaline ORR on Au(100).[52] We have demonstrated in our previous study of Pt(111) that the cationic effect is due to the cross sphere nature of reaction 4: it involves $OH^-$ in the outer sphere, which is sensitive to the cation solvated in the outer sphere. Our current AIMD simulations demonstrate the corollary on Au(100): with $OH^-$ stabilized by hydrogen bond interaction with Au(100) in the inner sphere, the rate for reaction 5 should be insensitive to the cation in the outer sphere, in agreement with the experiment.[52]

With a barrier of 0.1−0.2 eV, OH* desorption should not be the rate-limiting step for ORR on Au(100). As its experimentally measured equilibrium potential is 1.1 V, OH* desorption does not determine the onset of the ORR current, which is stopped at 1.0 V.[46] The role of OH* desorption in the overall ORR mechanism on Au(100) is quite different from that on Pt(111) and should be an interesting subject for further study.[53] It is also well-established that the equilibrium potential for OH* desorption on Pt(111), close to 1.0 V,[54] is lower than that on Au(100). The Au−OH interaction being weaker than the Pt−OH interaction is one obvious factor. The stabilization effect of the $OH^-\cdots Au$ hydrogen bond could be another factor. On Pt(111), OH* desorption is known to be the key step that determines the onset electrode potential of ORR in an alkaline medium.[24] On Au(100), OH* desorption is more facile and can reach a higher equilibrium electrode potential. As the $OH^-\cdots Au$ interaction is due to the intrinsic property of Au atoms, such hydrogen bonds should also be present on other gold surfaces or electrodes doped and/or alloyed with gold.

In conclusion, $OH^-$ can be a hydrogen bond donor to Au on Au(100), and the $OH^-\cdots Au$ hydrogen bond is stable even when a small amount of positive charge is added to the slab. It places the functioning of such a hydrogen bond in the ORR region, in contrast to the $Au\cdots H_2O$ hydrogen bond in the HER region, and points to a fundamental difference in the ORR mechanism between Au and Pt electrodes.

## ■ COMPUTATIONAL DETAILS

All molecular dynamics calculations are performed with the Vienna ab initio package (VASP).[55,56] The total energy and forces are calculated within the framework of density functional theory, which has been widely used in problems such as water autoionization[57−59] and $OH^-$ solvation.[36,39] The PBE exchange-correlation functional is employed,[60] with the dispersion interaction corrected by the D3 scheme.[61] The cutoff energy for the plane waves is 400 eV, and the atomic core region is described by PAW pseudopotentials.[62] The Γ point is used to integrate the Brillouin zone, and dipole correction along the $z$ direction is also added.[63]

Au(100) is modeled by a 4 × 4 surface slab of three layers, with the bottom two layers in fixed positions. With spaces available above a 4 × 4 surface for the expected structural fluctuation in the solution layer, such a model has been employed in recent AIMD studies of electrochemical reactions.[64−68] Previous studies have also shown that good accuracy in the dissociation energy of $H_2O$,[69] the physisorption energy of $H_2O$,[70] and the chemisorption energy of O[71] can be obtained with three layers, which saves computational cost so that a solution layer could be added to the surface. The lengths of $a$ and $b$ are both 11.75 Å, optimized from the unit cell of Au metal, while the length of $c$ is elongated to 39.15 Å, leaving enough space for an interfacial liquid layer of water molecules and a 20 Å vacuum region. There are originally 48 water molecules, arranged in a standard ice structure on the slab and relaxed by thermal annealing for 10 000 time steps. It is further optimized to reduce the forces on atoms to 0.02 eV/Å. In molecular dynamics simulations, the hydrogen mass is set to 2 amu and the time step is 1.2 fs. The simulation temperature is set to 300 K and controlled by a Nose-Hoover thermostat.[72−74] A similar setup is employed for the study of the Pt(111) electrode, with the same parameters as in our previous study.[24]

Metadynamics is a method for accelerating the sampling of reactive paths with an activation barrier.[75,76] A collective variable (CV) that defines the coordinate of a reaction is first selected, and bias Gaussian hills are successively added during an AIMD simulation. The potential well for the reactants is filled as the simulation progresses, facilitating the pushing over of the system to the potential well of the products. For example, in this study, we use a Au−OH* distance as the CV to facilitate the desorption of OH* to $OH^-$. The overall Hamiltonian evolves during a simulation run as

$$\tilde{H} = H + V_{\text{bias}}$$

where $H$ is the initial Hamiltonian and $V_{\text{bias}}$ is time-dependent and defined as the summation of all of the Gaussian hills added in previous steps

$$V_{\text{bias}} = h \sum_{i=1}^{[t/t_G]} \exp\left[-\frac{|\xi^{(t)} - \xi^{(it_G)}|^2}{2\omega^2}\right]$$

where $h$ is the Gaussian height, $\omega$ the Gaussian width, $t_G$ the frequency to add the Gaussian function, and $\xi$ the collective variable (i.e., the reaction coordinate). The parameters are as follows: $h$ = 0.03, $\omega$ = 0.1, and $t_G$ = 25 (obtained after trial runs). $V_{\text{bias}}$ also provides the free energy curve, as a function of the CV, from which the free energy barrier for the reaction can be obtained. For more details of our metadynamic simulations, see part D of the Supporting Information.

## ■ ASSOCIATED CONTENT

### Supporting Information

The Supporting Information is available free of charge at https://pubs.acs.org/doi/10.1021/acs.jpclett.2c02774.

Additional results and a discussion of electron-localized function, the relationship between the electrode potential and added charge, interaction energy between the hydrated $OH^-$ cluster and Au(100), and metadynamics of OH* desorption (PDF)

## ■ AUTHOR INFORMATION

### Corresponding Authors

**Yan-Xia Chen** − *Hefei National Research Center for Physical Sciences at Microscale, Department of Chemical Physics, University of Science and Technology of China, Hefei 230026, China;* orcid.org/0000-0002-1370-7422; Email: yachen@ustc.edu.cn

**Zhi-Feng Liu** − *Department of Chemistry and Centre for Scientific Modeling and Computation, Chinese University of Hong Kong, Shatin 999077 Hong Kong, China; CUHK Shenzhen Research Institute, Nanshan District, Shenzhen 518057, China;* orcid.org/0000-0002-6898-075X; Email: zfliu@cuhk.edu.hk

Author

**Yuke Li** − *Department of Chemistry and Centre for Scientific Modeling and Computation, Chinese University of Hong Kong, Shatin 999077 Hong Kong, China*

Complete contact information is available at: https://pubs.acs.org/10.1021/acs.jpclett.2c02774

## Notes

The authors declare no competing financial interest.

## ■ ACKNOWLEDGMENTS

This study is supported by the Research Grants Council of Hong Kong SAR Government (GRF Grant 14303114), the National Natural Science Foundation of China (22172151), and the Ministry of Science and Technology of China (G2022200006L). The authors are grateful for the generous allocation of computer time on the HPC clusters at the Center for Scientific Modeling and Computation. Some of the simulations were performed at the Shanghai Supercomputer Center.

## ■ REFERENCES

(1) Brammer, L. Metals and hydrogen bonds. *Dalton Trans.* **2003**, 3145−3157.
(2) Martín, A. Hydrogen Bonds Involving Transition Metal Centers Acting As Proton Acceptors. *J. Chem. Educ.* **1999**, *76*, 578.
(3) Schmidbaur, H.; Raubenheimer, H. G.; Dobrzanska, L. The gold-hydrogen bond, Au-H, and the hydrogen bond to gold, Au···HX. *Chem. Soc. Rev.* **2014**, *43*, 345−380.
(4) Schmidbaur, H. Proof of Concept for Hydrogen Bonding to Gold, Au···H-X. *Angew. Chem., Int. Ed.* **2019**, *58*, 5806−5809.
(5) Berger, R. J. F.; Schoiber, J.; Monkowius, U. A Relativity Enhanced, Medium-Strong Au(I)···H−N Hydrogen Bond in a Protonated Phenylpyridine-Gold(I) Thiolate. *Inorg. Chem.* **2017**, *56*, 956−961.
(6) Rigoulet, M.; Massou, S.; Sosa Carrizo, E. D.; Mallet-Ladeira, S.; Amgoune, A.; Miqueu, K.; Bourissou, D. Evidence for genuine hydrogen bonding in gold(I) complexes. *Proc. Natl. Acad. Sci. U.S.A.* **2019**, *116*, 46−51.
(7) Straka, M.; Andris, E.; Vicha, J.; Ruzicka, A.; Roithova, J.; Rulisek, L. Spectroscopic and Computational Evidence of Intramolecular $Au^{I}\cdots H^{+}-N$ Hydrogen Bonding. *Angew. Chem., Int. Ed* **2019**, *58*, 2011−2016.
(8) Abu Bakar, M.; Sugiuchi, M.; Iwasaki, M.; Shichibu, Y.; Konishi, K. Hydrogen bonds to Au atoms in coordinated gold clusters. *Nat. Commun.* **2017**, *8*, 576.
(9) Darmandeh, H.; Loffler, J.; Tzouras, N. V.; Dereli, B.; Scherpf, T.; Feichtner, K. S.; Vanden Broeck, S.; Van Hecke, K.; Saab, M.; Cazin, C. S. J.; Cavallo, L.; Nolan, S. P.; Gessner, V. H. Au···H-C Hydrogen Bonds as Design Principle in Gold(I) Catalysis. *Angew. Chem., Int. Ed.* **2021**, *60*, 21014−21024.
(10) Groenewald, F.; Dillen, J.; Raubenheimer, H. G.; Esterhuysen, C. Preparing Gold(I) for Interactions with Proton Donors: The Elusive [Au]···HO Hydrogen Bond. *Angew. Chem., Int. Ed.* **2016**, *55*, 1694−1698.
(11) Groenewald, F.; Raubenheimer, H. G.; Dillen, J.; Esterhuysen, C. Gold setting the "gold standard" among transition metals as a hydrogen bond acceptor − a theoretical investigation. *Dalton Trans.* **2017**, *46*, 4960−4967.
(12) Kumar, M.; Francisco, J. S. Evidence of the Elusive Gold-Induced Non-classical Hydrogen Bonding in Aqueous Environments. *J. Am. Chem. Soc.* **2020**, *142*, 6001−6006.
(13) Zheng, W.; Li, X.; Eustis, S.; Grubisic, A.; Thomas, O.; de Clercq, H.; Bowen, K. Anion photoelectron spectroscopy of $Au^{-}(H_2O)_{1,2}$, $(D_2O)_{1-4}$, and $AuOH^{-}$. *Chem. Phys. Lett.* **2007**, *444*, 232−236.
(14) Gao, Y.; Huang, W.; Woodford, J.; Wang, L. S.; Zeng, X. C. Detecting weak interactions between $Au^{-}$ and gas molecules: a photoelectron spectroscopic and ab initio study. *J. Am. Chem. Soc.* **2009**, *131*, 9484−9485.
(15) Park, G.; Gabbai, F. P. The Elusive Au(I)···H−O Hydrogen Bond: Experimental Verification. *J. Am. Chem. Soc.* **2021**, *143*, 12494−12498.
(16) Chen, Y. X.; Zou, S. Z.; Huang, K. Q.; Tian, Z. Q. SERS studies of electrode/electrolyte interfacial water part II - Librations of water correlated to hydrogen evolution reaction. *J. Raman Spectrosc.* **1998**, *29*, 749−756.
(17) Wu, D. Y.; Duan, S.; Liu, X. M.; Xu, Y. C.; Jiang, Y. X.; Ren, B.; Xu, X.; Lin, S. H.; Tian, Z. Q. Theoretical study of binding interactions and vibrational Raman spectra of water in hydrogen-bonded anionic complexes: $(H_2O)_n^{-}$ (n = 2 and 3), $H_2O\cdots X^{-}$ (X = F, Cl, Br, and I), and $H_2O\cdots M^{-}$ (M = Cu, Ag, and Au). *J. Phys. Chem. A* **2008**, *112*, 1313−1321.
(18) Chen, Y. X.; Otto, A. Electronic effects in SERS by liquid water. *J. Raman Spectrosc.* **2005**, *36*, 736−747.
(19) Ataka, K.; Yotsuyanagi, T.; Osawa, M. Potential-dependent reorientation of water molecules at an electrode/electrolyte interface studied by surface-enhanced infrared absorption spectroscopy. *J. Phys. Chem.* **1996**, *100*, 10664−10672.
(20) Li, C. Y.; Le, J. B.; Wang, Y. H.; Chen, S.; Yang, Z. L.; Li, J. F.; Cheng, J.; Tian, Z. Q. In situ probing electrified interfacial water structures at atomically flat surfaces. *Nat. Mater.* **2019**, *18*, 697−701.
(21) Schmickler, W. The transfer coefficient in proton transfer reactions. *J. Electroanal. Chem.* **1990**, *284*, 269−277.
(22) Li, Y.; Liu, Z. F. Modeling the effect of an anion on the free energy surfaces along the reaction pathways of oxygen reduction on Pt(111). *Chem. Phys. Lett.* **2019**, *736*, 136813.
(23) Li, Y.; Liu, Z. F. Solvated proton and the origin of the high onset overpotential in the oxygen reduction reaction on Pt(111). *Phys. Chem. Chem. Phys.* **2020**, *22*, 22226−22235.
(24) Li, Y.; Liu, Z. F. Cross-Sphere Electrode Reaction: The Case of Hydroxyl Desorption during the Oxygen Reduction Reaction on Pt(111) in Alkaline Media. *J. Phys. Chem. Lett.* **2021**, *12*, 6448−6456.
(25) Xantheas, S. S. Theoretical Study of Hydroxide Ion-Water Clusters. *J. Am. Chem. Soc.* **1995**, *117*, 10373−10380.
(26) Bader, R. F. Principle of stationary action and the definition of a proper open system. *Phys. Rev. B Condens. Matter* **1994**, *49*, 13348−13356.
(27) Savin, A.; Nesper, R.; Wengert, S.; Fässler, T. F. ELF: The Electron Localization Function. *Angew. Chem., Int. Ed.* **1997**, *36*, 1808−1832.
(28) Contreras-Garcia, J.; Johnson, E. R.; Keinan, S.; Chaudret, R.; Piquemal, J. P.; Beratan, D. N.; Yang, W. NCIPLOT: a program for plotting non-covalent interaction regions. *J. Chem. Theory Comput.* **2011**, *7*, 625−632.
(29) Johnson, E. R.; Keinan, S.; Mori-Sanchez, P.; Contreras-Garcia, J.; Cohen, A. J.; Yang, W. Revealing noncovalent interactions. *J. Am. Chem. Soc.* **2010**, *132*, 6498−506.
(30) Taylor, C. D.; Wasileski, S. A.; Filhol, J. S.; Neurock, M. First principles reaction modeling of the electrochemical interface: Consideration and calculation of a tunable surface potential from atomic and electronic structure. *Phys. Rev. B* **2006**, *73*, 165402.
(31) Filhol, J. S.; Neurock, M. Elucidation of the electrochemical activation of water over Pd by first principles. *Angew. Chem., Int. Ed.* **2006**, *45*, 402−406.
(32) Hamelin, A. Harmony of Electrochemical Results, in Situ STM Observations and in Situ SXRS Data, at Gold Faces - Aqueous Solution Interfaces. In *Nanoscale Probes of the Solid/Liquid Interface*; Gewirth, A. A., Siegenthaler, H., Eds.; Springer Netherlands: Dordrecht, The Netherlands, 1995; pp 285−306.
(33) Lust, E. Zero Charge Potentials and Electrical Double Layer at Solid Electrodes. In *Encyclopedia of Interfacial Chemistry*; Wandelt, K., Ed.; Elsevier: Oxford, U.K., 2018; pp 316−344.
(34) Velasco-Velez, J. J.; Wu, C. H.; Pascal, T. A.; Wan, L. F.; Guo, J.; Prendergast, D.; Salmeron, M. Interfacial water. The structure of

interfacial water on gold electrodes studied by x-ray absorption spectroscopy. *Science* **2014**, *346*, 831−834.
(35) Marx, D.; Chandra, A.; Tuckerman, M. E. Aqueous Basic Solutions: Hydroxide Solvation, Structural Diffusion, and Comparison to the Hydrated Proton. *Chem. Rev.* **2010**, *110*, 2174−2216.
(36) Agmon, N.; Bakker, H. J.; Campen, R. K.; Henchman, R. H.; Pohl, P.; Roke, S.; Thaemer, M.; Hassanali, A. Protons and Hydroxide Ions in Aqueous Systems. *Chem. Rev.* **2016**, *116*, 7642−7672.
(37) Robertson, W. H.; Diken, E. G.; Price, E. A.; Shin, J. W.; Johnson, M. A. Spectroscopic determination of the $OH^-$ solvation shell in the $OH^-\cdot(H_2O)_n$ clusters. *Science* **2003**, *299*, 1367−1372.
(38) Lin, R. J.; Nguyen, Q. C.; Ong, Y. S.; Takahashi, K.; Kuo, J.-L. Temperature dependent structural variations of $OH^-(H_2O)_n$, n = 4−7: effects on vibrational and photoelectron spectra. *Phys. Chem. Chem. Phys.* **2015**, *17*, 19162−19172.
(39) Crespo, Y.; Hassanali, A. Unveiling the Janus-Like Properties of $OH^-$. *J. Phys. Chem. Lett.* **2015**, *6*, 272−278.
(40) Crespo, Y.; Hassanali, A. Characterizing the local solvation environment of $OH^-$ in water clusters with AIMD. *J. Chem. Phys.* **2016**, *144*, 074304.
(41) Aziz, E. F.; Ottosson, N.; Faubel, M.; Hertel, I. V.; Winter, B. Interaction between liquid water and hydroxide revealed by core-hole de-excitation. *Nature* **2008**, *455*, 89−91.
(42) Corridoni, T.; Sodo, A.; Bruni, F.; Ricci, M. A.; Nardone, M. Probing water dynamics with $OH^-$. *Chem. Phys.* **2007**, *336*, 183−187.
(43) Walrafen, G. E.; Douglas, R. T. W. Raman spectra from very concentrated aqueous NaOH and from wet and dry, solid, and anhydrous molten, LiOH, NaOH, and KOH. *J. Chem. Phys.* **2006**, *124*, 114504.
(44) Sakong, S.; Forster-Tonigold, K.; Gross, A. The structure of water at a Pt(111) electrode and the potential of zero charge studied from first principles. *J. Chem. Phys.* **2016**, *144*, 194701.
(45) Huang, J. Surface charging behaviors of electrocatalytic interfaces with partially charged chemisorbates. *Curr. Opin. Electrochem.* **2022**, *33*, 100938.
(46) Mei, D.; He, Z. D.; Zheng, Y. L.; Jiang, D. C.; Chen, Y. X. Mechanistic and kinetic implications on the ORR on a Au(100) electrode: pH, temperature and H-D kinetic isotope effects. *Phys. Chem. Chem. Phys.* **2014**, *16*, 13762−13773.
(47) Ignaczak, A.; Santos, E.; Schmickler, W. Oxygen reduction reaction on gold in alkaline solutions - The inner or outer sphere mechanisms in the light of recent achievements. *Curr. Opin. Electrochem.* **2019**, *14*, 180−185.
(48) Quaino, P.; Luque, N. B.; Nazmutdinov, R.; Santos, E.; Schmickler, W. Why is gold such a good catalyst for oxygen reduction in alkaline media? *Angew. Chem., Int. Ed.* **2012**, *51*, 12997−3000.
(49) Staszak-Jirkovský, J.; Subbaraman, R.; Strmcnik, D.; Harrison, K. L.; Diesendruck, C. E.; Assary, R.; Frank, O.; Kobr, L.; Wiberg, G. K. H.; Genorio, B.; Connell, J. G.; Lopes, P. P.; Stamenkovic, V. R.; Curtiss, L.; Moore, J. S.; Zavadil, K. R.; Markovic, N. M. Water as a Promoter and Catalyst for Dioxygen Electrochemistry in Aqueous and Organic Media. *ACS Catal.* **2015**, *5*, 6600−6607.
(50) Lu, F.; Zhang, Y.; Liu, S.; Lu, D.; Su, D.; Liu, M.; Zhang, Y.; Liu, P.; Wang, J. X.; Adzic, R. R.; Gang, O. Surface Proton Transfer Promotes Four-Electron Oxygen Reduction on Gold Nanocrystal Surfaces in Alkaline Solution. *J. Am. Chem. Soc.* **2017**, *139*, 7310−7317.
(51) Strmcnik, D.; Kodama, K.; van der Vliet, D.; Greeley, J.; Stamenkovic, V. R.; Markovic, N. M. The role of non-covalent interactions in electrocatalytic fuel-cell reactions on platinum. *Nat. Chem.* **2009**, *1*, 466−472.
(52) Strmcnik, D.; van der Vliet, D. F.; Chang, K. C.; Komanicky, V.; Kodama, K.; You, H.; Stamenkovic, V. R.; Markovic, N. M. Effects of $Li^+$, $K^+$, and $Ba^{2+}$ Cations on the ORR at Model and High Surface Area Pt and Au Surfaces in Alkaline Solutions. *J. Phys. Chem. Lett.* **2011**, *2*, 2733−2736.
(53) Chen, W.; Huang, J.; Wei, J.; Zhou, D.; Cai, J.; He, Z.-D.; Chen, Y. X. Origins of high onset overpotential of oxygen reduction reaction at Pt-based electrocatalysts: A mini review. *Electrochem. commun.* **2018**, *96*, 71−76.
(54) Gomez-Marin, A. M.; Rizo, R.; Feliu, J. M. Oxygen reduction reaction at Pt single crystals: a critical overview. *Catal. Sci. Technol.* **2014**, *4*, 1685−1698.
(55) Kresse, G.; Hafner, J. *Ab initio* molecular-dynamics simulation of the liquid-metal-amorphous-semiconductor transition in germanium. *Phys. Rev. B Condens. Matter* **1994**, *49*, 14251−14269.
(56) Kresse, G.; Furthmüller, J. Efficiency of ab-initio total energy calculations for metals and semiconductors using a plane-wave basis set. *Comput. Mater. Sci.* **1996**, *6*, 15−50.
(57) Trout, B. L.; Parrinello, M. The dissociation mechanism of $H_2O$ in water studied by first-principles molecular dynamics. *Chem. Phys. Lett.* **1998**, *288*, 343−347.
(58) Geissler, P. L.; Dellago, C.; Chandler, D.; Hutter, J.; Parrinello, M. Autoionization in liquid water. *Science* **2001**, *291*, 2121−2124.
(59) Joutsuka, T. Molecular Mechanism of Autodissociation in Liquid Water: *Ab Initio* Molecular Dynamics Simulations. *J. Phys. Chem. B* **2022**, *126*, 4565−4571.
(60) Perdew, J. P.; Burke, K.; Ernzerhof, M. Generalized Gradient Approximation Made Simple. *Phys. Rev. Lett.* **1996**, *77*, 3865−3868.
(61) Grimme, S.; Antony, J.; Ehrlich, S.; Krieg, H. A consistent and accurate *ab initio* parametrization of density functional dispersion correction (DFT-D) for the 94 elements H-Pu. *J. Chem. Phys.* **2010**, *132*, 154104.
(62) Kresse, G.; Joubert, D. From ultrasoft pseudopotentials to the projector augmented-wave method. *Phys. Rev. B* **1999**, *59*, 1758−1775.
(63) Neugebauer, J.; Scheffler, M. Adsorbate-substrate and adsorbate-adsorbate interactions of Na and K adlayers on Al(111). *Phys. Rev. B Condens. Matter* **1992**, *46*, 16067−16080.
(64) Cheng, T.; Goddard, W. A.; An, Q.; Xiao, H.; Merinov, B.; Morozov, S. Mechanism and kinetics of the electrocatalytic reaction responsible for the high cost of hydrogen fuel cells. *Phys. Chem. Chem. Phys.* **2017**, *19*, 2666−2673.
(65) Ye, Y. F.; Yang, H.; Qian, J.; Su, H. Y.; Lee, K. J.; Cheng, T.; Xiao, H.; Yano, J.; Goddard, W. A.; Crumlin, E. J. Dramatic differences in carbon dioxide adsorption and initial steps of reduction between silver and copper. *Nat. Commun.* **2019**, *10*, 1875.
(66) Cheng, T.; Xiao, H.; Goddard, W. A. Full atomistic reaction mechanism with kinetics for CO reduction on Cu(100) from ab initio molecular dynamics free-energy calculations at 298 K. *Proc. Natl. Acad. Sci. U.S.A.* **2017**, *114*, 1795−1800.
(67) Xiao, H.; Cheng, T.; Goddard, W. A.; Sundararaman, R. Mechanistic Explanation of the pH Dependence and Onset Potentials for Hydrocarbon Products from Electrochemical Reduction of CO on Cu (111). *J. Am. Chem. Soc.* **2016**, *138*, 483−486.
(68) Goldsmith, Z. K.; Calegari Andrade, M. F.; Selloni, A. Effects of applied voltage on water at a gold electrode interface from *ab initio* molecular dynamics. *Chem. Sci.* **2021**, *12*, 5865−5873.
(69) Wang, J. G.; Hammer, B. Density functional theory study of water dissociation in a double water bilayer with or without coadsorption of CO on Pt(111). *J. Chem. Phys.* **2006**, *124*, 184704.
(70) Nadler, R.; Sanz, J. F. Effect of dispersion correction on the Au(111)-$H_2O$ interface: A first-principles study. *J. Chem. Phys.* **2012**, *137*, 114709.
(71) Malek, A.; Eikerling, M. H. Chemisorbed Oxygen at Pt(111): a DFT Study of Structural and Electronic Surface Properties. *Electrocatalysis* **2018**, *9*, 370−379.
(72) Nosé, S. A unified formulation of the constant temperature molecular dynamics methods. *J. Chem. Phys.* **1984**, *81*, 511−519.
(73) Hoover, W. G. Canonical dynamics: Equilibrium phase-space distributions. *Phys. Rev. A* **1985**, *31*, 1695−1697.
(74) Nosé, S. Constant Temperature Molecular Dynamics Methods. *Prog. Theor. Phys. Suppl.* **1991**, *103*, 1−46.
(75) Laio, A.; Gervasio, F. L. Metadynamics: a method to simulate rare events and reconstruct the free energy in biophysics, chemistry and material science. *Rep. Prog. Phys.* **2008**, *71*, 126601.


https://doi.org/10.1021/acs.jpclett.2c02774
J. Phys. Chem. Lett. 2022, 13, 9035−9043

(76) Bucko, T. *Ab initio* calculations of free-energy reaction barriers. *J. Condens. Matter Phys.* **2008**, *20*, 064211.





https://doi.org/10.1021/acs.jpclett.2c02774
*J. Phys. Chem. Lett.* 2022, 13, 9035−9043